EPJ Web of Conferences **3**, 04019 (2010)
DOI:10.1051/epjconf/20100304019

Tensor optimized shell model using bare interaction for light nuclei

Takayuki Myo[1,2,a], Hiroshi Toki[2], and Kiyomi Ikeda[3]

[1] Osaka Institute of Technology, Osaka, Osaka 535-8585, Japan
[2] Research Center for Nuclear Physics, Osaka University, Ibaraki, Osaka 567-0047, Japan
[3] RIKEN Nishina Center, Wako, Saitama 351-0198, Japan.

Abstract. We propose a new theoretical approach to calculate nuclear structure using bare nuclear interaction, in which the tensor and short-range correlations are described by using the tensor optimized shell model (TOSM) and the unitary correlation operator method (UCOM), respectively. We compare the obtained results using TOSM+UCOM for ^{4}He with the rigorous calculation. We also apply TOSM to the analysis of two-neutron halo nuclei, ^{6}He and ^{11}Li, on the basis of the "core with TOSM"+n+n model. The halo formation of ^{11}Li is explained by inclusion of the tensor correlation in ^{9}Li core, which produces the Pauli-blocking on the p-wave neutrons in ^{11}Li and enhances the s-wave component of halo structure.

1 Introduction

It is important to develop a theoretical framework to calculate nuclear structure using bare nucleon-nucleon interaction. Recently it becomes possible to calculate nuclei up to mass around $A \sim 12$ by using the Green's Function Monte-Carlo method[1]. The binding energies of nuclei were successfully reproduced by including three body interaction. One big surprise is a large contribution of the one-pion exchange interaction, which is about 70∼80 % of the whole bare interaction. It is however extremely time consuming to apply this method to heavier nuclei. It is desired to develop a new method to calculate nuclei with large nucleon numbers by using the bare interaction.

The nucleon-nucleon interaction has distinctive features, namely there exist strong tensor interaction at intermediate distance caused by pion exchange and strong short-range repulsive interaction at a short distance caused by quark dynamics. Although these two interactions have totally different characteristics, it is customary to adopt the theory, such as the Brueckner Hartree-Fock, to integrate out the high-momentum components emerging from the tensor interaction and short-range repulsion on the same footing. In this way, one loses direct information on the tensor correlation and a short-range correlation in the wave function. Hence, we search for a powerful method of treating treat explicitly both the tensor interaction and the short-range interaction to study of not only light nuclei but also medium and heavy nuclei.

There are two important developments for this purpose. One is to find out that the tensor interaction is of intermediate range. We are able to express the tensor correlation in a reasonable shell model space[2–4]. We name this method as Tensor Optimized Shell Model (TOSM), where the wave function is constructed in terms of the shell model basis states with full optimization of the two particle-two hole ($2p2h$) states. We have shown that the tensor interaction could be treated by taking a reasonable amount of multipoles ($l \leq 5$) for the particle states[2].

The other is the Unitary Correlation Operator Method (UCOM) for the treatment of the short-range correlation[5, 6]. We shall combine two methods, TOSM and UCOM (TOSM + UCOM), to describe nuclei using bare interaction. We hope to apply a newly developed method to many nuclei[4]. We use TOSM for the strong tensor interaction utilizing the intermediate nature caused by finite angular momentum of the relative wave function, and use UCOM for the strong short-range interaction utilizing the short-range nature. Using TOSM+UCOM, we aim to understand the roles of the tensor and short-range correlations in nuclei using bare interaction. As a good start, we apply TOSM+UCOM to ^{4}He and compare the obtained results with rigorous calculations[7] and see how this method works by using bare interaction and how far we can describe each correlations and to find what we are supposed to do for further improvement.

We have also investigated the characteristics of the tensor correlations in He and Li isotopes, such as the p-wave doublet splitting energy in ^{5}He and ^{6}He[8,9], the mechanisms of the inversion phenomenon in ^{10}Li and the neutron halo formation in ^{11}Li[3]. In particular, so far, the problem of the neutron halo formation in ^{11}Li is still unclear. The halo structure of ^{11}Li has a large $(1s)^2$ component of last two neutrons, indicating the magic number breaking of $N = 8$. The mechanism to explain this exotic phenomena of ^{11}Li has been not explained theoretically. We solved this problem of the $N = 8$ shell gap by treating the tensor correlation explicitly in TOSM. Based on the three-body model with the ^{9}Li core described in TOSM, the Pauli-blocking for the tensor correlation in core produces the energy loss for the p-wave configuration of ^{10,11}Li. As a

[a] e-mail: myo@ge.oit.ac.jp

result, the magic number breaking in ^{11}Li was naturally explained[3].

2 Tensor Optimized Shell Model (TOSM)

We explain the framework of TOSM. We shall begin with many-body Hamiltonian,

$$H = \sum_i T_i - T_{\rm c.m.} + \sum_{i<j} V_{ij}, \tag{1}$$

$$V_{ij} = v_{ij}^C + v_{ij}^T + v_{ij}^{LS} + v_{ij}^{Clmb}\ . \tag{2}$$

Here, T_i is the kinetic energy of each nucleons with $T_{\rm c.m.}$ being the center of mass term. We take the bare interaction for V_{ij} such as AV8′ consisting of central (v_{ij}^C), tensor (v_{ij}^T) and spin-orbit (v_{ij}^{LS}) terms. v_{ij}^{Clmb} is the Coulomb term. We obtain the many-body wave function Ψ with the equation, $H\Psi = E\Psi$.

We begin with the TOSM wave function. We write the case of ^{4}He explicitly as an example including the variational coefficients $\{A_k\}$.

$$\Psi = A_0|0\rangle + \sum_{k=1} A_k|2p2h\rangle_k, \tag{3}$$

$$|2p2h\rangle_k = |[[\psi_{n_1\alpha_1}(\mathbf{x}_1), \psi_{n_2\alpha_2}(\mathbf{x}_2)]^J \tag{4}$$

$$\otimes [\tilde{\psi}_{n_3\alpha_3}(\mathbf{x}_1), \tilde{\psi}_{n_4\alpha_4}(\mathbf{x}_2)]^J]^0\rangle \tag{5}$$

Here, $|0\rangle$ is $|(0s)^4\rangle$ for ^{4}He. $|2p2h\rangle$ are the $2p2h$ states with various radial components. k denotes representable quantum number of $2p2h$ states using the single particle (hole) wave functions $\psi_{n,\alpha}$ ($\tilde{\psi}_{n,\alpha}$) with the quantum numbers n and α; n is an index to distinguish the different radial wave functions. α are the sets of the spin-isospin quantum numbers to distinguish the single particle orbits. We describe the the various radial wave functions of single particle orbits by using the Gaussian expansion method[2, 10].

We explain the Gaussian expansion technique for single-particle orbits. Each Gaussian basis function has the form of a nodeless harmonic oscillator wave functions (HOWF), except for $1s$ orbit. When we superpose a sufficient number of Gaussian bases with various length parameters, we can fully optimize the radial component of every orbit of every configuration with respect to the total Hamiltonian in Eq. (1). We construct the following ortho-normalized single-particle wave function ψ_α^n with a linear combination of Gaussian bases $\{\phi_\alpha\}$ with length parameter $b_{\alpha,\nu}$.

$$\psi_\alpha^n(\mathbf{r}) = \sum_{\nu=1}^{N_\alpha} d_{\alpha,m}^n\, \phi_\alpha(\mathbf{r}, b_{\alpha,\nu}) \tag{6}$$

$$\text{for } n = 1, \cdots, N_\alpha, \tag{7}$$

where N_α is a number of basis functions for the orbit α, and ν is an index that distinguishes the bases with different values of $b_{\alpha,\nu}$. The explicit form of the Gaussian basis function is expressed as

$$\phi_\alpha(\mathbf{r}, b_{\alpha,\nu}) = N_l(b_{\alpha,\nu})\, r^l\, e^{-(r/b_{\alpha,\nu})^2/2}\, [Y_l(\hat{\mathbf{r}}), \chi_{1/2}^\sigma]_j \chi_{t_z}, \tag{8}$$

$$N_l(b_{\alpha,\nu}) = \left[\frac{2\, b_{\alpha,\nu}^{-(2l+3)}}{\Gamma(l+3/2)}\right]^{\frac{1}{2}}, \tag{9}$$

where l and j are the orbital and total angular momenta of the single-particle states, respectively, and t_z is the projection of the nucleon isospin. The coefficients $\{d_{\alpha,\nu}^n\}$ are determined by solving the eigenvalue problem for the norm matrix of the non-orthogonal Gaussian basis set in Eq. (8) with the dimension N_α. Following this procedure, we obtain new single-particle wave functions $\{\psi_\alpha^n\}$ in Eq. (7) for TOSM.

We choose the Gaussian bases for the particle states to be orthogonal to the occupied single-particle states, which are $0s_{1/2}$ in the ^{4}He case. For $0s_{1/2}$ states, we employ one Gaussian basis function, namely, HOWF with length $b_{0s_{1/2},\nu=1} = b_{0s}$. For $1s_{1/2}$ states, we introduce an extended $1s$ basis function orthogonal to the $0s_{1/2}$ states and possessing a length parameter $b_{1s,\nu}$ that differs from b_{0s} [2]. In the extended $1s$ basis functions, we change the polynomial part from the usual $1s$ basis states to satisfy the conditions of the normalization and the orthogonality to the $0s$ state.

Two-body matrix elements in the Hamiltonian are analytically calculated using the Gaussian bases[2, 10], whose explicit forms are given in Appendix of Ref. [4] for central, LS and tensor interactions, respectively. In the numerical calculation, we prepare 9 Gaussian functions at most with various range parameters to get a convergence of the energy.

We have to furthermore take care of the center-of-mass excitations. For this aim, we take the well-tested method of introducing a center-of-mass term in the many body Hamiltonian[11].

$$H_{\rm cm} = \lambda \left(\frac{\boldsymbol{P}_{\rm cm}^2}{2A\,m} + \frac{1}{2}\,A\,m\,\omega^2\,\boldsymbol{R}_{\rm cm}^2 - \frac{3}{2}\hbar\omega\right), \tag{10}$$

$$\boldsymbol{P}_{\rm cm} = \sum_{i=1}^{A} \boldsymbol{p}_i, \quad \boldsymbol{R}_{\rm cm} = \frac{1}{A}\sum_{i=1}^{A} \boldsymbol{r}_i, \tag{11}$$

$$\omega = \frac{\hbar}{m\, b_{0s}^2}, \tag{12}$$

where m and A are the nucleon mass and the mass number, respectively, and b_{0s} is the length parameter of HOWF for the hole $0s$ state. We take sufficiently large coefficient, λ, to project out only the lowest HO state for the center-of-mass motion. In the numerical calculation, the excitation of the spurious center-of-mass motion is suppressed to be less than 10 keV.

The variation of the energy expectation value with respect to the total wave function Ψ is given by

$$\delta \frac{\langle\Psi|H|\Psi\rangle}{\langle\Psi|\Psi\rangle} = 0\,, \tag{13}$$

which leads to the following equations:

$$\frac{\partial\langle\Psi|H-E|\Psi\rangle}{\partial b_{\alpha,\nu}} = 0\,, \tag{14}$$

$$\frac{\partial\langle\Psi|H-E|\Psi\rangle}{\partial A_k} = 0\,. \tag{15}$$

Here, E is a Lagrange multiplier corresponding to the total energy. The parameters $\{b_{\alpha,\nu}\}$ for the Gaussian bases appear in non-linear forms in the energy expectation value.

We solve two kinds of variational equations in the following steps. First, fixing all the length parameters $b_{\alpha,\nu}$, we solve the linear equation for $\{A_k\}$ as an eigenvalue problem for H with partial waves up to $L_{\max}$. We thereby obtain the eigenvalue E, which is a function of $\{b_{\alpha,\nu}\}$. Next, we try to search various sets of the length parameters $\{b_{\alpha,\nu}\}$ in order to find the solution which minimizes the total energy. In this TOSM wave function, we can describe the spatial shrinkage with an appropriate radial form, which is important for the tensor correlation[2].

3 Unitary Correlation Operator Method (UCOM)

We present UCOM for the short-range correlation[5,6], in which the following unitary operator is introduced

$$C = \exp(-i \sum_{i<j} g_{ij}) = \prod_{i<j} c_{ij}, \tag{16}$$

$$c_{ij} = \exp(-i\, g_{ij}). \tag{17}$$

We express the correlated wave function, Ψ, in terms of less sophisticated wave function, Φ, as $\Psi = C\Phi$. Hence, the Schrödinger equation becomes $\hat{H}\Phi = E\Phi$ where $\hat{H} = C^\dagger HC$. Since C is expressed with a two-body operator in the exponential, it is a many-body operator. In the case of the short-range correlation, we are able to truncate modified operators at the level of two-body operators[5].

We define the two-body Hermite operator g in Eq. (17) as

$$g = \frac{1}{2}\{p_r s(r) + s(r) p_r\}, \tag{18}$$

$$\frac{dR_+(r)}{dr} = \frac{s(R_+(r))}{s(r)}, \tag{19}$$

where p_r is the radial component of the relative momentum, which is conjugate to the relative coordinate r. $s(r)$ is the amount of the shift of the relative wave function and depending on r. In UCOM, we use $R_+(r)$ instead of $s(r)$. The function $R_+(r)$ corresponds to the transformed relative coordinate from r, and represents the correlation function to reduce the amplitude of the short-range part of the relative wave functions. The explicit transformation of the operator for the relative motion is given as $c^\dagger r c = R_+(r)$ for example[5]. We use TOSM to describe Φ.

In the calculation using UCOM, we parametrize R_+(r) in the same manner as proposed by Neff-Feldmeier and Roth et al.[5,6,12]. We assume the following forms for even and odd channels, respectively.

$$R_+^{\rm even}(r) = r + \alpha \left(\frac{r}{\beta}\right)^\gamma \exp[-\exp(r/\beta)], \tag{20}$$

$$R_+^{\rm odd}(r) = r + \alpha\,(1 - \exp(-r/\gamma))\exp[-\exp(r/\beta)]. \tag{21}$$

Here, α, β, γ are the variational parameters to optimize the function $R_+(r)$ and minimize the energy of the system. They are independently determined for four channels of the spin-isospin pair. In the actual procedure of the variation, once we fix the parameters included in $R_+(r)$, we solve the eigenvalue problem of the Hamiltonian using Eq. (15) and determine the configuration mixing of the shell model-type bases in TOSM. Next, we try to search various sets of the $R_+(r)$ parameters to minimize the obtained energy.

3.1 Extension of UCOM –S-wave UCOM–

In the framework of UCOM, we introduce the UCOM function $R_+(r)$ for each spin-isospin channel and ignore the partial wave dependence of $R_+(r)$. It is generally possible to introduce the partial wave dependence in UCOM and then $R_+(r)$ functions are determined in each relative partial wave in the two-body matrix elements. Here, we consider the specific case of this extension of UCOM by taking care of the characteristics of the short range correlation. One of the simplest case of this extension is UCOM for only s-wave relative motion. Since all the other partial waves l except for s-wave ($l = 0$) have r^l behavior near at the origin, this r^l behavior cuts down the effect of the short range hard core largely. However, only the s-wave function is finite at the origin and the behavior in the origin is determined by the hard core dynamics. In fact, the method used by Feldmeier et al. is to determine the unitary operator in order to reproduce the short range behavior of s-wave relative wave function[5].

When we incorporate S-wave UCOM (S-UCOM, hereafter) into TOSM, we extract the relative s-wave component in every two-body matrix elements in TOSM using the V type basis expanded by the Gaussian functions. For numerical calculations, we prepare the completeness relation consisting of the T type basis functions $|T\rangle$ as

$$1 = \sum_i |T_i\rangle\langle T_i|, \tag{22}$$

$$|T_i\rangle = |[[\psi_l^{\boldsymbol{r}}\psi_L^{\boldsymbol{R}}]_{L'}, \chi_S\,]_J\,\chi_T\rangle, \tag{23}$$

where the T type basis is expanded by the two coordinates of the relative part $\boldsymbol{r}$ and the center of mass part $\boldsymbol{R}$ of two nucleons, which are the set of Jacobi coordinate. The orbital angular momenta of each coordinate, $\boldsymbol{r}$ and $\boldsymbol{R}$ are l and L, respectively. It is easy to prepare the s-wave relative part by putting l to be zero in the T type basis. We construct the above completeness relation of the T type basis states by diagonalizing the norm matrix expanded by the finite number of the Gaussian basis functions for two coordinates. In the actual calculation, we use 12 bases for each coordinate, with which convergence is achieved.

We calculate the matrix elements of the arbitrary two-body operator $\hat{O}$ including the S-UCOM correlator C_s using the V type basis with indices α and β. Here, we insert the above T type completeness relation in Eq. (23) as

$$\langle V_\alpha|C_s^\dagger\hat{O}C_s|V_\beta\rangle = \sum_{ij}\langle V_\alpha|T_i\rangle\langle T_i|C_s^\dagger\hat{O}C_s|T_j\rangle\langle T_j|V_\beta\rangle. \tag{24}$$

The matrix element using T type base, $\langle T_i|C_s^\dagger\hat{O}C_s|T_j\rangle$ is calculated for the two-body kinetic part and central, ten-

Table 1. Optimized parameters in $R_+(r)$ in TOSM+UCOM for four channels in fm in the present work.

	α	β	γ
singlet even	1.32	0.88	0.36
triplet even	1.33	0.93	0.41
singlet odd	1.57	1.26	0.73
triplet odd	1.18	1.39	0.53

sor interactions. For the kinetic part and the central interaction, the matrix elements conserve the relative angular momentum, and then we can easily calculate the matrix elements of the transformed operator $C_s^\dagger \hat{O} C_s$. For the tensor interaction, the *sd* coupling matrix elements are properly treated, in which C_s is operated on only the *s*-wave part of the relative motion. In this case, the operator C_s acts on the *s*-wave relative Gaussian basis function $\phi_{l=0}(r)$, which is transformed as

$$C_S\ \phi_{l=0}(r) = \frac{R_-(r)}{r}\ \sqrt{R'_-(r)}\,\phi_{l=0}(R_-(r)), \qquad (25)$$

where $R_-(r)$ is the inverse transformation of $R_+(r)$, namely $R_-(R_+(r)) = r$. The matrix elements of the T type basis function are calculated using the above transformed wave function. We also calculate the overlap between V type and T type bases using Gaussian basis functions, whose explicit form is given in the appendix of Ref. [4].

4 Variational calculation of ^{4}He in TOSM+UCOM

First, we determine the UCOM functions $R_+(r)$ for the calculation of TOSM+UCOM. We optimize $R_+(r)$ function by changing the three parameters of α, β and γ to search for the energy minimum in TOSM+UCOM. In Table 1, the optimized three parameters in S-UCOM are listed. The adopted $R_+(r)$ in UCOM for four channels are shown in Fig. 1. The demonstration of the calculated result to search for the energy minimum is shown in Fig. 2. In Fig. 2, the total energy is plotted as a function of the range parameter, β of $R_+(r)$ function in Eq. (20) for the triplet even channel in the case of $L_{\max}$ being 10. We have already minimized α and γ for each β in this calculation. We see clearly a desired behavior, where the energy has a minimum as a function of β. Hence, we fix β that provides the lowest energy.

We show the calculated results for the energy of ^{4}He in Fig. 3, where $L_{\max}$ is the maximum orbital angular momentum of the particle states. In Fig. 3, we get a good convergence of the energy with respect to $L_{\max}$. We show two results using UCOM and S-UCOM. The latter S-UCOM is the extended UCOM, in which the UCOM transformation is performed only for the relative *s*-wave component of the even channel, while the original UCOM does not consider any partial wave dependence. In UCOM, it is found that the binding energy of ^{4}He is underestimated. The reason are understood as due to too large removal of the short-range part of the relative wave functions, in particular, in the *d*-wave part of the *sd* coupling of the tensor matrix element, where the tensor interaction possesses some amount of strength. We have also calculated the contributions beyond the $2p2h$ configurations in TOSM such as $3p3h$ and $4p4h$ configurations. When we include the $4p4h$ configurations within the *p*-shell, their contribution to the binding energy is approximately 50 keV. This fact denotes that these more complicated wave functions contribute very little in the total ^{4}He wave function.

In order to overcome this feature of UCOM, we have decided to restrict the use of UCOM to the relative *s*-wave only for the even channel (S-UCOM), where the treatment of the short-range repulsion is absolutely necessary. In other partial waves, we have the centrifugal potential that cuts out the short-range part from the wave functions of the higher partial waves. In this case, we can use the transformed interaction and the kinetic energy only for the relative *s*-wave component in the even channels. Since the use of the UCOM for the odd partial wave is slightly better, we use the UCOM for all odd partial waves. we have introduced S-UCOM and found that the situation was largely improved to give about 23 MeV of the binding energy. The tensor force contribution also gains by about 5 MeV in comparison with the one using UCOM. This gain mainly

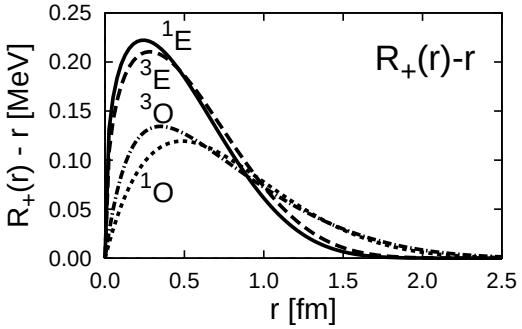

Fig. 1. The UCOM functions $R_+(r)$ used in even ($^{1,3}E$) and odd ($^{1,3}O$) channels. The differenes between $R_+(r)$ and the original coordinate r are displayed.

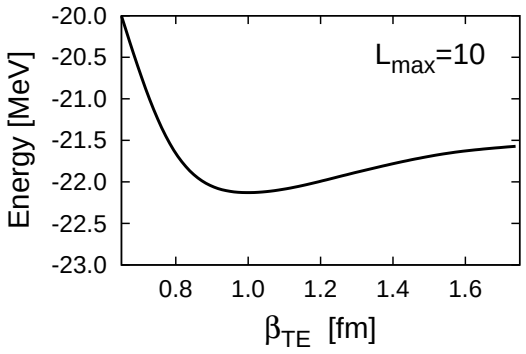

Fig. 2. Energy surface of ^{4}He with respect to β of triplet even channel with $L_{\max}$ being 10.

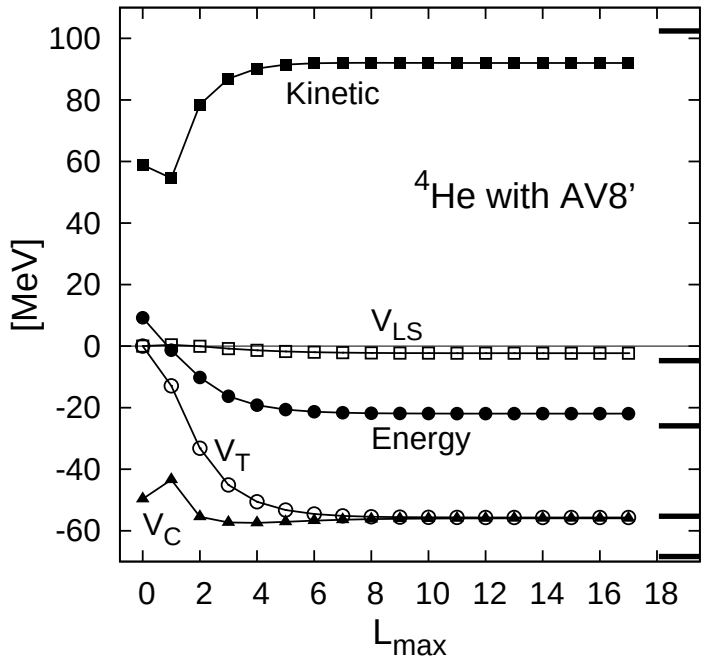

Fig. 4. Matrix elements of the central interaction (V_C), tensor interaction (V_T) and the spin-orbit interaction (V_{LS}) together with the kinetic energy (Kinetic) and total energy (Energy) in the Hamiltonian using AV8′ for ^{4}He as function of $L_{\max}$. These values are compared with the benchmark results of Ref. [7], which are indicated by the thick short solid lines on the right-hand side of the figure.

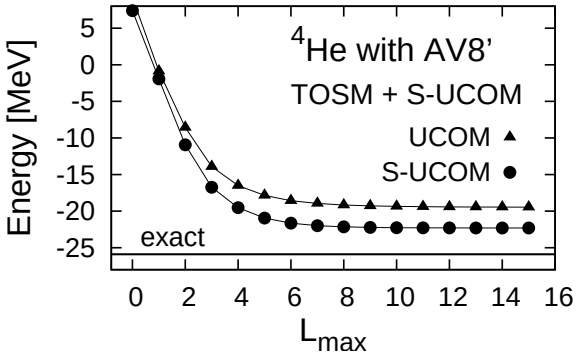

Fig. 3. Energy of ^{4}He in TOSM + UCOM / S-UCOM. Exact calculation is taken from Ref. [7].

comes from the *sd* coupling matrix elements of the tensor force.

As for the comparison with the rigorous calculation, we see that v^C agrees with the rigorous value, about 55 MeV. On the other hand, the tensor matrix element, v^T converges to 55 MeV, while the rigorous one is 68 MeV. The kinetic energy is about 90 MeV, while the rigorous one is 102 MeV. The spin orbit matrix element is also smaller than the rigorous value. As the net value, the total energy is 23 MeV which is close to the rigorous value 26 MeV. One of the possibilities for the lack of the energy in TOSM + (S)-UCOM is due to the separate treatment of the short-range and tensor correlations. Although the dominant part of the tensor interaction is of intermediate and long range, there may remain some small strength in the short-range part of the tensor interaction, which can couple with the short-range correlations. This effect can be included by extending the truncation of the UCOM transformation in the Hamiltonian to more than the two-body level. Three-body term of the UCOM transformation is one of the possibilities to overcome the lack of energy in TOSM+UCOM[5]. This term can contribute to increase the tensor matrix element and produce the high momentum component in the wave function.

To see the properties of the obtained ^{4}He wave function, the dominant configurations are listed in Table 2 with their probabilities. It is found that the several $2p2h$ states such as $(0s)^{-2}_{10}(0p_{1/2})^2_{10}$ are largely mixed and those configurations are essential for the tensor correlation in ^{4}He[2, 13]. It is also found that the $0p0h$-$2p2h$ coupling exhausts 94% of the tensor matrix element.

We show now all the components of the energy for ^{4}He in Fig. 4. All the energy components show the saturation behavior as function of $L_{\max}$. In the tensor component, the saturation is obtained at around $L_{\max}$ being 8. For the other components, their saturation points are seen at the similar $L_{\max}$. A very interesting feature is the kinetic energy, which goes up to a large value as the tensor interaction matrix element becomes large. As for the comparison with the rigorous calculation, we see that V_c satisfies the rigorous value, which is approximately −55 MeV. On the other hand, the tensor interaction matrix element, V_T converges to −55 MeV, while the rigorous one is −68 MeV. The kinetic energy is approximately 90 MeV, while the rigorous one is 102 MeV. The LS matrix element is also smaller than the rigorous value. As the net value, the total energy, E, is −23 MeV and the rigorous value is −26 MeV.

Table 2. Mixing probabilities in the ^{4}He ground state in %, where two subscripts of 00 and 10 are the spin-isospin quantum numbers.

$(0s)^4_{00}$	83.01
$(0s)^{-2}_{10}(0p_{1/2})^2_{10}$	2.45
$(0s)^{-2}_{10}[(1s_{1/2})(0d_{3/2})]_{10}$	2.31
$(0s)^{-2}_{10}[(0p_{3/2})(0f_{5/2})]_{10}$	1.90
$(0s)^{-2}_{10}[(0p_{1/2})(0p_{3/2})]_{10}$	1.45
$(0s)^{-2}_{10}[(0d_{5/2})(0g_{7/2})]_{10}$	0.80
$(0s)^{-2}_{10}(0d_{3/2})^2_{10}$	0.48
remaining part	7.60

5 Tensor correlation in neutron halo nuclei

In this section, we discuss the effect of tensor correlation in halo nuclei ^{6}He and ^{11}Li. It is shown that in ^{4}He, there exists the selection rule of the particle states in the $2p2h$ configurations, coupled by the tensor force. In particular, the $0p_{1/2}$ component is largely mixed, as shown in Table 2. It is interesting to investigate the coupling between ^{4}He core nucleus and halo neutrons in ^{6}He. Similarly the ^{11}Li case with ^{9}Li+n+n system can be considered. For this purpose, we employ the three-body cluster model of halo nuclei with core+n+n, in which the core nucleus is described using TOSM.

5.1 Three-body model of halo nuclei with TOSM core

The Hamiltonian of two-neutron halo nuclei with core+n+n system is given in the orthogonality condition model[3]

$$H = H(\text{core}) + \sum_{i=1}^{3} T_i - T_G + \sum_{i=1}^{2} V_{cn,i} + V_{nn}, \quad (26)$$

where H(core), T_i and T_G are the internal Hamiltonian of core given in Eq. (1), the kinetic energies of each cluster and the center-of-mass of the three-body system, respectively. The microscopic core-n potential, V_{cn}, is given by a folding-type one[3,9]. AV8′ is used for the last two neutrons. We remove the Pauli forbidden states for the core-n relative motion, which depends on the configuration of core in TOSM, including $2p2h$ states[8,3]. We slightly adjust the strength of the core-n potential to reproduce the observed two-neutron separation energies of ^{6}He and ^{11}Li, respectively. We do not introduce any conventional partial-wave dependence, such as the deep s-wave ^{9}Li-n potential for ^{11}Li.

The wave function of two-neutron halo nuclei with the spin J is given as

$$\Psi^J = \sum_k \mathcal{A}\left\{ [\Phi^{J_c}_k, \chi^j_k(nn)]^J \right\}, \quad (27)$$

where J_c and j are the spins of the core configuration $\Phi^{J_c}_k$ and the coupled last two neutrons, respectively. The two-neutron wave function $\chi^j_k(nn)$ is exactly obtained in a few-body technique. The wave function of subsystem such as ^{5}He and ^{10}Li are similarly given in a coupled two-body problem of the core+n system.

5.2 ^{6}He

We investigate the effect of tensor correlation in ^{6}He. As for ^{5}He, the subsystem of ^{6}He, the effect of the tensor force has been shown to have the dependence of orbital states occupied by the last neutron. Terasawa[14–16] and Nagata et al.[17] performed the configuration mixing for the ^{4}He part. The internal excitation of ^{4}He causes the Pauli blocking in ^{5}He, which produces the orbital-state dependence. Thus, this effect is responsible for some amount of the observed doublet splitting of p-wave states[8].

Here, we reanalyze the doublet splitting of p-waves in ^{6}He within an extended ^{4}He+n+n model[9], where we explicitly take into account the tensor correlation in the ^{4}He cluster in TOSM. The $(0s)^2(0p_{1/2})^2$ configurations are strongly suppressed due to the Pauli principle between a valence neutron of $p_{1/2}$-wave and $0p_{1/2}$ orbital neutrons in the ^{4}He, as shown in Fig. 5. Thus, we investigate to what extent the tensor correlation of ^{4}He generates the Pauli blocking and results in the doublet splitting of p-waves in ^{6}He.

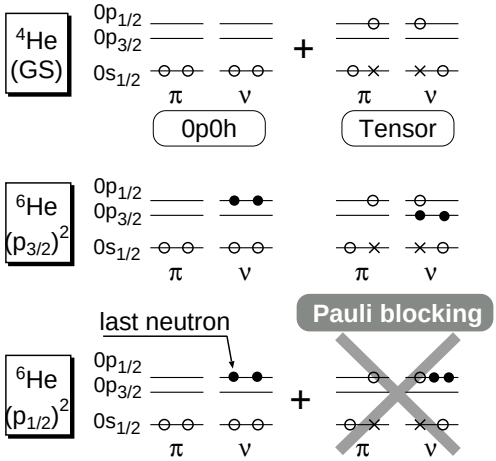

Fig. 5. Pauli-blocking effects of tensor correlations in ^{6}He.

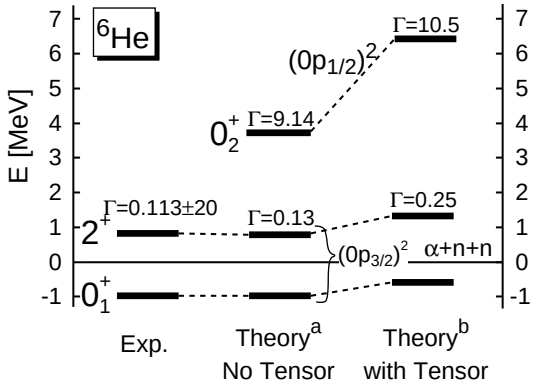

Fig. 6. Results of ^{6}He spectra w/o (a) and with (b) the tensor correlation. The energy is measured from the α threshold.

We obtain the ^{6}He spectra in the coupled ^{4}He+n+n model in Fig. 6.Resonances are treated by using the complex scaling method. Due to the large mixing of $0p_{1/2}$ component from the tensor correlation in ^{4}He, the Pauli blocking strongly occurs in the 0^+_2 state of ^{6}He in which two valence neutrons occupy the $0p_{1/2}$ orbit and suppress the tensor correlation in the ^{4}He core due to the Pauli-principle. On the other hand, the ground state of ^{6}He is dominated by $(p_{3/2})^2$ configuration for halo neutrons with about 90%, then the blocking effect is small. As a result, the splitting from the ground state becomes large[9], which is the theoretical prediction.

5.3 ^{11}Li

We explain the essential point of the model for Li isotopes to incorporate the tensor correlation, whose details were given in the Refs. [3,25]. We start from ^{9}Li with TOSM. Instead of UCOM, we here use the G-matrix effective force, which retains the strong tensor force of the AV8′ bare NN force, and adjust the central force to reproduce the observed binding energy of ^{9}Li[3]. In TOSM, we consider up to the $2p2h$ excitations within the p shell in TOSM. This treatment does not change the characteristics of the tensor and pairing correlations, and also the essential results obtained for Li isotopes. In TOSM, we adopt the spatially modified harmonic oscillator basis as a single particle orbit and treat their length parameters independently and variationally to optimize the tensor correlation.

We show the results of the ^{9}Li in TOSM, where b_{0s} and $b_{0p_{3/2}}$ are optimized as 1.45 fm and 1.8 fm. For $0p_{1/2}$-orbit, we superpose two bases with different length of $b_{0p_{1/2}}$ as 0.85 fm and 1.8 fm. This is to describe both the tensor and pairing correlations, since the tensor correlation is optimized with spatially shrunk excited nucleons and the pairing correlation is optimized with the spatially extended orbits[3]. Among the $2p2h$ configurations, the large components are given by $(0p_{3/2})^{-2}_{01}(0p_{1/2})^2_{01}$ with 9.0 % for the pairing correlation and $(0s)^{-2}_{10}(0p_{1/2})^2_{10}$ with 7.2 % for the tensor one. The subscripts 01 or 10 represent spin and isospin for the two-nucleon pair, respectively. The tensor force contribution is −20.7 MeV. The charge radius of ^{9}Li is 2.23 fm, which reproduces the experiments (2.217 ± 0.035[18]).

We consider the dynamical effect of the tensor and pairing correlations on the structures of ^{11}Li. When we add two neutrons to ^{9}Li, the $2p2h$ excitations induced by two correlations in ^{9}Li are blocked by the last neutrons under the Pauli-principle. In Fig. 7, we show this Pauli-blocking effect on the $(0p)^2$ and $(1s)^2$ configurations in ^{11}Li. For the $(0p)^2$ case (middle panel), the $2p2h$ excitation in ^{9}Li is suppressed and the ^{9}Li energy is lost inside ^{11}Li[3,25]. For the $(1s)^2$ case (lower panel), the Pauli-blocking does not occur and ^{9}Li part gains its energy by the configuration mixing with the $2p2h$ excitations. Hence, the relative energy distance between two configurations of ^{11}Li can become small, which reduces the shell gap. The same blocking effect is similarly taken into account in ^{10}Li.

Table 3. Various r.m.s. radius of ^{11}Li.

	Present	Expt.
$R_{\rm matter}$ [fm]	3.41	3.12±0.16[20]
		3.53±0.06[21]
		3.71±0.20[22]
$R_{\rm charge}$	2.44	2.467±0.037[18]
$R_{n\text{-}n}$	7.33	

Table 4. p-wave resonances in ^{10}Li, where E_r and Γ are the resonance energy measured from the ^{9}Li+n threshold and the decay width. The value a_s is the s-state scattering length of the ^{9}Li+n system.

$(E_r, \Gamma)(1^+)$ [MeV]	(0.22, 0.09)
$(E_r, \Gamma)(2^+)$ [MeV]	(0.64, 0.45)
$a_s(1^-)$ [fm]	−5.6
$a_s(2^-)$ [fm]	−17.4

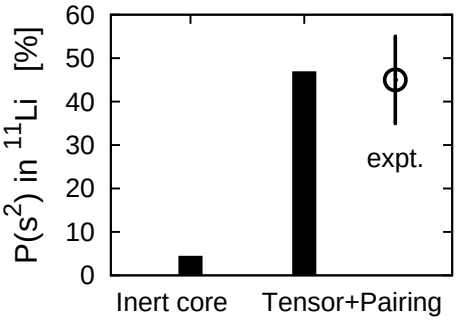

Fig. 8. $(1s)^2$ probability in ^{11}Li in comparison with the experiment[19].

We perform the coupled three-body calculation to obtain $\Psi^J(^{11}\text{Li})$ in Eq. (27). In Fig. 8, our present calculation "Tensor+Pairing" gives 46.9% of the $(1s)^2$ probability $P(s^2)$ for ^{11}Li, which explains the observations[19]. The probabilities of $(p_{1/2})^2$, $(p_{3/2})^2$, $(d_{5/2})^2$ and $(d_{3/2})^2$ for the last two neutrons are obtained as 42.7%, 2.5%, 4.1% and 1.9%, respectively. For comparison, we calculate ^{11}Li without core excitations of ^{9}Li ("Inert Core"), namely, we adopt only the single $0p0h$ configuration for ^{9}Li without the Pauli-blockings explained in the middle panel of Fig. 7. In that case, ^{11}Li has almost p-shell closed configuration of 90.6% with a small $P(s^2)$ of 4.3%. In the present model of "Tensor+Pairing", the energy difference between $(1s)^2$ and $(0p_{1/2})^2$ configurations is estimated as −0.1 MeV, which is enough to couple two configurations by the pairing correlation between the last two neutrons. This means that the blocking effect of the tensor and pairing correlations are essential for the breaking of magicity in ^{11}Li. The tensor effect is found to be stronger than the pairing one[3].

We show the results of the various radii of ^{11}Li in Table 3. Our result gives a large matter radius $R_{\rm matter}$ for ^{11}Li, due to a large value of $P(s^2)$ for halo neutrons. The charge radius ($R_{\rm charge}$) is also reproduced well. The enhancement

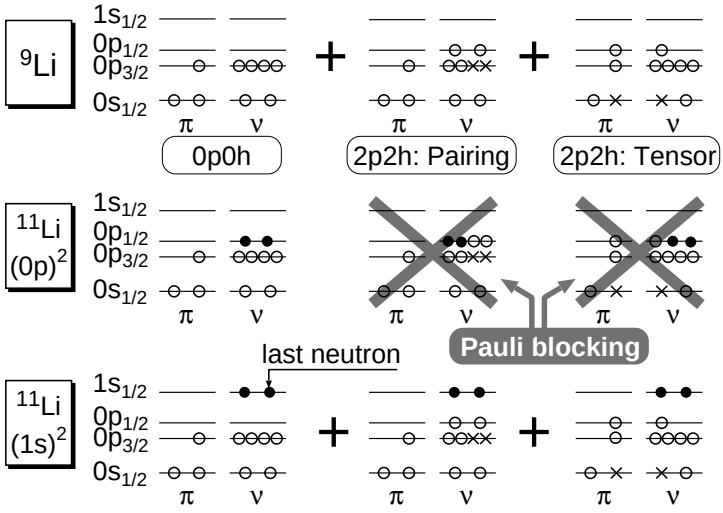

Fig. 7. Pauli-blocking effects of tensor and pairing correlations in ^{11}Li.

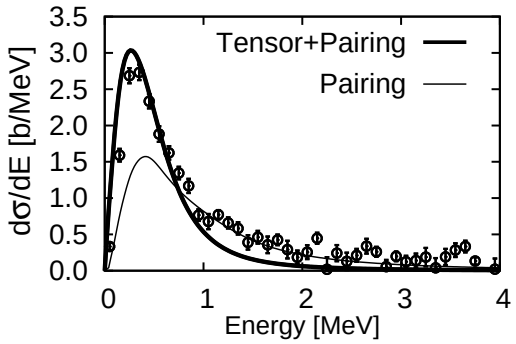

Fig. 9. Three-body Coulomb breakup cross section of ^{11}Li measured from the ^{9}Li+n+n threshold energy. Pairing case is taken from Ref. [23].

of charge radius from that of ^{9}Li is mainly caused by the large distance between ^{9}Li and the paired two neutrons, R_{c-2n}, obtained as 5.69 fm[3]. This is a recoil effect.

We further investigate the unbound states of ^{10}Li. In Table 4, the dual p state resonances coupled with the spin of ^{9}Li$(3/2^-)$ are obtained near the ^{9}Li+n threshold energy. For the s states, the ^{9}Li+n scattering lengths, a_s, show negative values. In particular, the 2^- state gives a large negative value of a_s, which indicates the virtual s state near the ^{9}Li+n threshold energy. Therefore the inversion phenomenon in ^{10}Li is explained in the present model.

We finally calculate the Coulomb breakup strength of ^{11}Li into the ^{9}Li+n+n system to investigate the properties of the dipole excited states. We cannot find any three-body resonance to make structures in the strength. In Fig. 9, the present model well reproduces the experiment[24], in particular, for low energy enhancement. Among the final state interactions, both of the core-n and nn interactions give comparable contributions to produce the low energy enhancement in the strength[25].

6 Summary

We have developed a method to calculate nuclear ground state by using the bare interaction in the tensor optimized shell model (TOSM+UCOM). We have treated the tensor interaction in terms of TOSM, in which the $2p2h$ states are fully optimized to describe the excitations due to the tensor interaction. As for the short-range repulsive interaction, we have introduced the unitary correlation operator method (UCOM). We have furthermore considered the extension of UCOM by introducing the partial wave dependence on the correlation function, named as S-UCOM, which largely improves the results.

We have also performed the systematic studies of halo nuclei, ^{6}He and ^{11}Li based on the extended core+n+n model. In the model, the tensor and pairing correlations are explicitly included for core nucleus using TOSM. For Li isotopes, the Pauli-blocking effect induced by two kinds of the correlations in ^{9}Li explains the halo structure of ^{11}Li and the inversion phenomena of ^{10}Li. The similar blocking effect can be seen in the excited 0^+_2 state of ^{6}He.

Acknowledgements

The authors are grateful to Prof. H. Horiuchi and Prof. K. Kat$\bar{\text{o}}$ for the fruitful discussions on the role of the tensor interaction on nuclear structure. This work was supported by a Grant-in-Aid for Young Scientists from the Japan Society for the Promotion of Science (JSPS, No. 21740194) and also by the JSPS Core-to-Core Program. Numerical calculations were performed on the computer system at RCNP, Osaka University.

References

1. S.C. Pieper and R. B. Wiringa, Annu. Rev. Nucl. Part. Sci. **51** (2001) 53.

2. T. Myo, S. Sugimoto, K. Katō, H. Toki, K. Ikeda, Prog. Theor. Phys. **117** (2007) 257.
3. T. Myo, K. Katō, H. Toki and K. Ikeda, Phys. Rev. **C76** (2007) 024305.
4. T. Myo, H. Toki, K. Ikeda, Prog. Theor. Phys. **121** (2009) 511.
5. H. Feldmeier, T. Neff, R. Roth and J. Schnack, Nucl. Phys. **A632** (1998) 61.
6. T. Neff and H. Feldmeier, Nucl. Phys. **A713** (2003) 227.
7. H. Kamada *et al.*, Phys. Rev. **C64** (2001) 044001.
8. T. Myo, K. Katō, K. Ikeda, Prog. Theor. Phys. **113** (2005) 763.
9. T. Myo, K. Katō, H. Toki, K. Ikeda, J. of Phys. **G31** (2005) S1681.
10. E. Hiyama, Y. Kino and M. Kamimura, Prog. Part. Nucl. Phys. **51** (2003) 223.
11. D.H. Gloeckner, R.D. Lawson, Phys. Lett. **B53** (1974) 313.
12. R. Roth, P. Papakonstantinou, N. Paar, H. Hergert, T. Neff and H. Feldmeier, Phys. Rev. **C73** (2006) 044312.
13. H. Toki, S. Sugimoto and K. Ikeda, Prog. Theor. Phys. **108** (2002) 903.
14. T. Terasawa, Prog. Theor. Phys. **22** (1959) 150.
15. T. Terasawa, Prog. Theor. Phys. **23** (1960) 87.
16. A. Arima and T. Terasawa, Prog. Theor. Phys. **23** (1960) 115.
17. S. Nagata, T. Sasakawa, T. Sawada and R. Tamagaki, Prog. Theor. Phys. **22** (1959) 274.
18. R. Sánchez *et al.*, Phys. Rev. Lett. **96** (2006) 033002.
19. H. Simon *et al.*, Phys. Rev. Lett. **83** (1999) 496.
20. I. Tanihata *et al.*, Phys. Lett. **B206** (1988) 592.
21. J. A. Tostevin and J. S. Al Khalili, Nucl. Phys. **A616** (1997) 418c.
22. A. V. Dobrovolsky *et al.*, Nucl. Phys. **A766** (2006) 1.
23. T. Myo, S. Aoyama, K. Katō, and K. Ikeda, Phys. Lett. **B576** (2003) 281.
24. T. Nakamura *et al.*, Phys. Rev. Lett. **96** (2006) 252502.
25. T. Myo, Y. Kikuchi, K. Katō, H. Toki and K. Ikeda, Prog. Theor. Phys. **119** (2008) 561.